

ASCA observation of Unusually X-ray Hard Radio Quiet QSO Kaz 102

Takamitsu MIYAJI¹, Yoshitaka ISHISAKI², Yoshihiro UEDA³, Yasushi OGASAKA⁴, Hisamitsu AWAKI⁵,
Kiyoshi HAYASHIDA⁶

¹*Department of Physics, Carnegie Mellon University, Pittsburgh, PA 15213, USA*
miyaji@cmu.edu

²*Department of Physics, Tokyo Metropolitan University, Minami Osawa 1-1, Hachioji, Tokyo 192-0397*
ishisaki@phys.metro-u.ac.jp

³*ISAS, 3-1-1 Yoshinodai, Sagamihara, Kanagawa 229-8510*
ueda@astro.isas.ac.jp

⁴*Department of Astrophysics, Nagoya University, Nagoya, Aichi 464-01*
ogasaka@u.phys.nagoya-u.ac.jp

⁵*Department of Physics, Ehime University, Matsuyama, Ehime 790-8577*
awaki@sgr.phys.sci.ehime-u.ac.jp

⁶*Department of Astrophysics, Osaka University, Matikane, Toyonaka, Osaka 560-0043*
hayasida@ess.sci.osaka-u.ac.jp

(Received ; accepted)

Abstract

We have observed a radio-quiet QSO Kaz 102 ($z=0.136$) with *ASCA* as a part of our program of complete spectral characterization of hard X-ray selected AGNs. We found that Kaz 102 shows unusual spectral properties. A simple power-law with absorption in our galaxy gave a satisfactory description of the spectrum. However, it showed a very hard photon index of $\Gamma \sim 1.0$ with no sign of deep absorption or a prominent spectral feature. We further explored the Compton reflection with Fe $K\alpha$ line and warm absorber models for hardening the spectra. Both gave statistically satisfactory fits. However, the Compton reflection model requires a very low metal abundance (0.03-0.07 in solar units). The warm absorber model with no direct component is preferred and gave a very high ionization parameter $\xi \sim 10^{2.3}$. If this is the case, the values of ξ , warm absorber column density, and variability over ~ 10 years may suggest that the warm absorber resides in the broad-line region and crosses the line of sight to the central X-ray source.

Key words: galaxies:active – galaxies: quasars: individual (Kaz 102=Q 1803+676) – X-rays:galaxies – X-rays:general

1. Introduction

The underlying intrinsic X-ray continua of AGNs without apparent deep absorption usually show a power-law form with a typical photon index of $\Gamma \sim 1.7 - 2.0$. There is some dispersion in the spectral indices, however. For example, Narrow-line Seyfert 1 galaxies (NLS1) are known to have intrinsically softer spectra, with up to $\Gamma \approx 2.5$ (e.g. Leighly 1999). AGNs with apparently much harder spectra usually arises from some reprocessing, i.e., absorption (by neutral or partially ionized gas) and/or Compton-reflection. These reprocessing leaves some characteristic features, which are sometimes hard to recognize in X-ray spectra with low signal-to-noise ratio.

As a part of our study of a complete determination of spectral properties of a hard X-ray selected bright AGNs using *ASCA* and *XMM-Newton* (Miyaji 2001), the primary goal of which is to serve as a bright-end constraint to hard X-ray luminosity function, evolution, and X-ray AGN population synthesis studies (e.g. Ueda et al. in preparation), we have observed a radio-quiet QSO (RQQ) Kaz 102 (a.k.a. 1803+676) with *ASCA*. The results of the study of the whole sample will be reported elsewhere

(Miyaji et al. in preparation).

Kaz 102 is an optically-bright RQQ at $z = 0.136$ with broad lines ($H\alpha$ FWHM ≈ 5000 km s⁻¹ (Treves et al. 1995; de Diego et al. 1998) and was already recognized as a very hard X-ray source with a photon index of $\Gamma \sim 0.8_{-0.4}^{+0.6}$, when it was observed by the *Einstein Observatory* in 1979 (Wilkes & Elvis 1987). However, during the *ROSAT* All-Sky Survey (RASS) in July 1990-January 1991, the spectral index in the *ROSAT* band was much softer ($\Gamma \sim 2.2$), which was typical of an RQQ in the *ROSAT* band (Cieliegi & Maccaacaro 1996; Treves et al. 1995). In this letter, we report the unusual spectral properties of this object during our *ASCA* observation. Luminosities are calculated using $H_0 = 65$ km s⁻¹Mpc⁻¹, $\Omega_m = 0.3$ and $\Omega_\Lambda = 0.7$.

2. ASCA Observation and Analysis

2.1. Observation

The *ASCA* observation was made during the *ASCA* AO7 period as a part of our larger program (see above). The log of observation of Kaz 102 is shown in Table 1. Data reduction and extraction of events have been made

Table 1. Log of *ASCA* observation of Kaz 102

Sequence	Obs. Date	Exposure	SIS/GIS Modes
77015000	Sep. 5, 1999	20 ks	1CCD-Faint/PH

using **FTOOLS 5.0** or later and spectral fittings have been made using **XSPEC 11.2**¹.

We found no significant variability of X-ray flux during the *ASCA* observation.

2.2. Spectral Extraction and Analysis

The SIS and GIS pulse-height spectra have been created from the events screened with the standard screening criteria. Background has been accumulated from the off-source area of the same observation for the SIS spectra. For the GIS spectra, we have used backgrounds from both the off-source area of the same observation and the standard-screened blank sky observation with a similar N_{H} value to that of our target location (using the **FTOOLS** task **mkgisbgd**). There was very little difference in the GIS results between these two background estimation methods, and thus we present the results with the background from the off-source area of the same observation. Spectra from two SISs (SIS0/SIS1) and the two GISs (GIS2/GIS3) have been co-added separately and the co-added SIS and GIS spectra have been analyzed jointly. We have made spectral analysis using pulse height channels corresponding to 1-7 keV and 0.7-9 keV for SIS and GIS respectively. We ignored SIS channels below 1 keV, where the responses are affected by radiation damage and there are calibration uncertainties associated with it for observations during late stages of the mission. In any event, because of the limited statistics, the impact of this effect, corresponding to a spurious excess absorption of $N_{\text{H}} \approx 5 \times 10^{20} \text{ cm}^{-2}$ (Yaqoob 2000), is not significant, as demonstrated by the upper limit to the extra absorption over the Galactic value (Sec. 2.2.1). All errors and upper limits correspond to a 90% confidence level ($\Delta\chi^2 = 2.7$). The unfolded GIS and SIS spectra corrected for the Galactic absorption are shown in Fig. 1 in the $E F(E)$ space. The spectra of previous X-ray observations, from *ROSAT* All-Sky Survey (Treves et al. 1995) and *Einstein* are also shown.

2.2.1. Single Power-Law and Galactic Absorption

Firstly we have tried to fit the *ASCA* GIS and SIS spectra with a single power-law. A Galactic absorption component, with the column density fixed to $N_{\text{H}} = 4.6 \times 10^{20} \text{ [cm}^{-2}\text{]}$, is included in all the spectral fittings in this and following subsections. The spectral slope was a joint parameter and the global normalizations were separate parameters. When additional neutral absorber located at the redshift of the object ($z = 0.136$) is added, we found a 90% upper limit of $N_{\text{H}}^z < 1.0 \times 10^{21} \text{ cm}^{-2}$. The result of the fit is under column (1) of Table 2, giving a photon

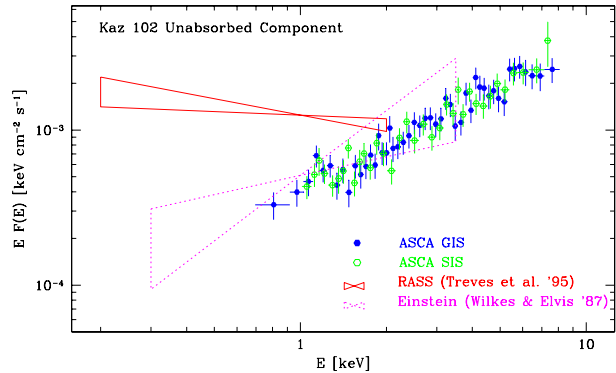


Fig. 1. The unfolded $E F(E)$ GIS and SIS spectra are shown with the results of the power-law fits of the *ROSAT* All-sky Survey (Treves et al. 1995) and *Einstein* (Wilkes & Elvis 1987) spectra.

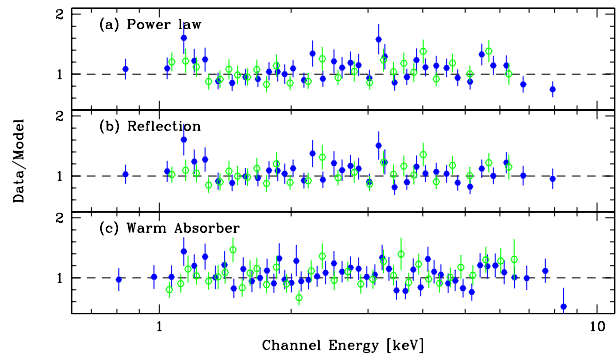


Fig. 2. The data/model ratios of the three spectral fits discussed in Sect. 2.2 are shown with 1σ errors.

spectral index of $\Gamma = 1.02 \pm .06$ with $\chi^2/\nu = 1.01$. The 2-10 keV luminosity at the object's rest frame is $L_x \approx 2.3 \times 10^{44} \text{ erg s}^{-1}$, which is the luminosity of a moderately powerful QSO. The residuals from the best-fit power-law model is shown in Fig. 2(a).

As seen in Fig. 2(a), we see a weak edge-feature at the object's rest frame of $E_{\text{ed}} = 1.5 \pm 0.1 \text{ keV}$ and $0.2 < \tau_{\text{ed}} < 0.7$ (90% confidence). A similar feature is seen in the *ASCA* spectrum of NGC 4395 (Iwasawa et al. 2000). Adding the edge improved the fit by $\Delta\chi^2 = 16$ with two additional degree of freedom (F-test probability of 5×10^{-3}).

2.2.2. Compton Reflection Model

We have tried to fit the spectrum of this AGN with a canonical $\Gamma = 1.9$ intrinsic power-law and an additional Compton reflection component. We tried **XSPEC** models for both the ionized (*pxriv*) and neutral (*pxrav*) reflectors (Magdziarz & Zdziarski 1995). The best-fit neutral reflector (*pxrav*) model with $\cos i = 0.45$ (fixed) gave $\chi^2/\nu = 0.95$, where $\pi/2 - i$ is the angle between the line of sight and the plane of the reflector surface. When a narrow Gaussian (width is fixed at 0.01 keV) is added at the redshifted Fe $K\alpha$ line energy of 5.6 keV (fixed), the fit has marginally improved with $\Delta\chi^2 = 3.6$ (F-test probability of 6%), while the values of other parameters did not

¹ <http://heasarc.gsfc.nasa.gov/docs/xanadu/xspec/>

change dramatically. The fit result in this case is shown in Table 2 column (2). Equally acceptable fits have been obtained for $\cos i$ values of 0.1 and 0.8 with almost the same χ^2 values, giving $rel_refl=6.5$ and 29 respectively.

In the *pearriv* fit, where the reflector temperature (T) and the ionization parameter (ξ , in units of $[\text{erg s}^{-1} \text{cm}]$ defined by Done et al. (1992)) are assumed to satisfy the equilibrium condition (see below), we only obtain an upper limit $\xi < 100$ ($T < 4 \times 10^5 \text{K}$) for $\cos i = 0.45$. Varying the values of ξ within this limit is compensated by the variation of rel_refl parameter and the normalization, where their best-fit values become $rel_refl \approx 21$, $S_{x12} = 0.5$ (direct component only) and abundance=0.1 at this upper limit.

The range of rel_refl indicates that one requires at least several times stronger source of incident radiation than that is seen as the direct component in order to produce the reflection component. This could be because some blocking material partially covers our line of sight to the original power-law source but the reflectors can be seen. Alternatively, the original source may have become fainter, while the reflected X-rays arrive later with extra paths.

The 90% confidence range of the Fe $K\alpha$ equivalent width (EW) from the fit was 10-290 eV. The abundance parameter of *pearriv* is constrained to be very low, with a 90% confidence range of 0.03-0.07 in solar units. With solar abundance, the data fail to fit with concavity around photon energies at 2-4 keV from a collection of numerous edges. The constraint from the single Fe K edge play a minor role because of the limited photon statistics at $E \gtrsim 6$ keV. At the position of the redshifted Fe $K\alpha$ emission line (5.6 keV), the reflection component dominates and Fig. 2 of Ballantyne, Fabian, & Ross (2002) can be used to find constraints from the Fe $K\alpha$ EW. At this low abundance, the EW of ~ 300 eV or lower is consistent with for all values of ξ . Conversely, this EW range corresponds to an Fe abundance of $\lesssim 0.2$ for a neutral reflector, but for our upper limit of ξ (~ 100) in equilibrium, the constraint becomes looser (Fe abundance $\lesssim 1$). Thus we cannot exclude the possibility that the X-ray emission of this object is reflection dominated from the spectral fit alone.

2.2.3. Warm Absorber Model

We have also considered a model with $\Gamma = 1.9$ intrinsic power-law (fixed), and a warm absorber, using the XSPEC model *absori* (Done et al. 1992; Zdziarski et al. 1995). One of the motivations of considering this is the existence of the absorption edge as described in Sect.2.2.1. The *absori* model does not include the solution for local radiative transfer and thermal-ionization balance, and it requests the absorber's temperature T and ionization parameter ξ as independent parameters. We have approximately solved for ξ and T as follows. These two parameters are strongly correlated and cannot be determined independently by the spectral fit. Thus we have first determined the best-fit ξ as a function of T . This is plotted in Fig. 3 as a solid line. We then overplot the ξ - T relation (dashed line) in the thermal-ionization equilibrium case from Fig. 4 of Reynolds & Fabian (1995) for the $\Gamma = 1.8$ ionization

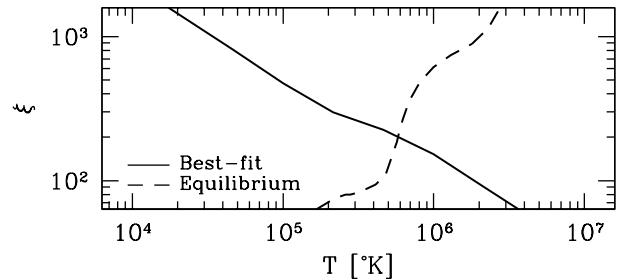


Fig. 3. Solid curve shows the best-fit ionization parameter ξ for given absorber temperatures T . The dashed curve show the condition where the absorbing gas is in equilibrium (Reynolds & Fabian 1995).

source, which is the closest to our assumption. These two curves give a solution of $(\xi, T) = (200, 6 \times 10^5 \text{K})$.

The fit result is shown under column (3) of Table 2, where ξ and T are jointly varied along the equilibrium line during the fit and error search. In this table, $N_{\text{H}22}^Z$ represents the column density of the warm absorber and the abundance is the iron abundance in solar units, and ξ is the ionization parameter. Indeed the best-fit warm absorber model gave a blend of edge features near $E \sim 1.5$ keV and the χ^2/ν value has been improved compared with the single power-law case partially because of this. A caveat is that the errors in these parameters represent only statistical errors of the fit under restrictive assumptions and should be treated accordingly. The analysis shows that if the warm absorber model is the case, the line of sight to the X-ray source is totally covered by a highly ionized ($\log_{10} \xi \sim 2.3$) slab of gas with a column density of $\approx 3 \times 10^{23} \text{cm}^{-2}$.

3. Discussion

Kaz 102 has an apparently unusual spectral property. Fig. 4 shows the histogram of the photon indices (Γ) of 28 of the ~ 50 AGNs in our sample (see Sect. 1) which seem unabsorbed, i.e., those which have intrinsic absorption of $N_{\text{H}} < 10^{21} \text{cm}^{-2}$ in the simple absorbed power-law fits. Fig. 4 shows the unusually small spectral index among these “unabsorbed” AGNs, and also harder than the range of spectral indices of 26 RQQs observed by George et al. (2000). It is also worth noting that this spectral index is difficult to produce with the current standard theory of AGN hard X-ray continuum involving inverse-Compton scattering by a hot corona (e.g. Haardt & Maraschi 1993). Thus this object deserves an individual attention.

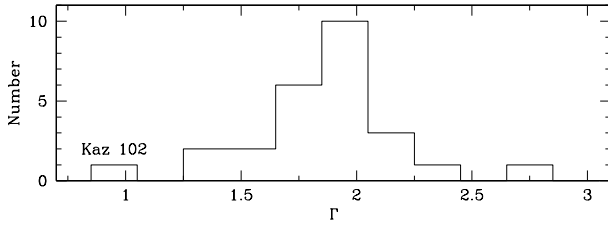
To understand the nature of this object better, we plot the infrared to hard X-ray spectral energy distribution (SED) of Kaz 102 in Fig. 5. For a comparison, the mean SED of radio-quiet QSOs (RQQ) (Elvis et al. 1994) normalized to the luminosity of this object at around $\lambda = 6000$ Å is overplotted. We see that the *ROSAT* spectrum is well on the mean RQQ SED.

From the three spectral fits shown in Sect. 2.2, we found statistically satisfactory fits in any case. We consider the reflection-dominated picture unlikely because the

Table 2. Results of the Spectral Fits

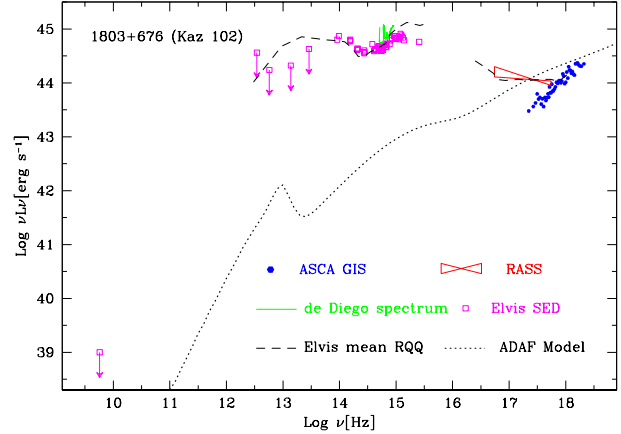
Parameter	PL (1)	Reflection (2)	Warm abs. (3)
Γ	$1.02 \pm .06$	1.9 (fixed)	1.9 (fixed)
$N_{\text{H}22}^z$ ^{a)}	< 0.1	...	34 ± 11
S_{x12}^{PL} ^{b)}	$4.8 \pm .3$	$.9 \pm .1$	$4.5 \pm .4$
$\log_{10} \xi$ ^{c)}	...	< 2.0	$2.3 \pm .1$
T [10^5 °K] ^{c)}	...	< 4	$5.8 \pm .4$
abundance	...	$.05 \pm .02$	$.2 \pm .1$
rel_refl	...	9.2 ± 1.3	...
EW(Fe) ^{d)}	...	150 ± 140	...
χ^2/ν	157./156	145./155	150./155

Notes: Galactic absorption is included in all models. All upper limits have been fixed to 0 for the determination and error search of other parameters. ^{a)} In units of 10^{22} [cm^{-2}]. This represents column densities of neutral and warm absorbers for columns (1) and (3) respectively. ^{b)} The *ASCA* GIS 2-10 keV flux in units of 10^{-12} [$\text{erg s}^{-1} \text{cm}^{-2}$]. This represents the fluxes of the intrinsic (before absorption) for (1) and (3) and of the direct component only for (2) respectively. ^{c)} T and ξ are linked assuming the equilibrium condition. See text. ^{d)} The equivalent width of the Fe $K\alpha$ line in eV in the object's frame.

**Fig. 4.** The distribution of the photon index Γ of *unabsorbed* AGNs in our hard X-ray selected sample (Miyaji 2001; Miyaji et al. in prep.) with Kaz 102 labeled.

fit requires unusually low heavy element abundance of less than 0.1 solar, which is much less than clusters/groups of galaxies and is not likely for gas in galaxies. We have also considered the possibility of accretion flow (ADAF) with a mass accretion rate \dot{m} close to the critical value \dot{m}_{crit} , above which ADAF solutions do not exist, as the origin of the hard X-ray emission. The X-ray portion of the calculated SEDs of the ADAF spectrum from Di Matteo (priv. comm) based on the model described in Di Matteo et al. (1999; 2003) are overplotted in Fig. 5 for $M_{\text{BH}} = 10^8 M_{\odot}$ and $\dot{m} = \dot{m}_{\text{crit}}$. These parameters are chosen to give approximately the luminosity of Kaz 102 at $E \sim 8$ keV. We see that the X-ray portion of this ADAF model ($\Gamma \sim 1.4$) is not hard enough to explain our *ASCA* X-ray spectrum of Kaz 102 and also fail to explain the optical-UV portion of the SED by a large factor. This is essentially due to the fact that we see the blue bump (BBB) in the UV region, which does not exist in the ADAF model.

The existence of the sign of an edge feature gives pref-

**Fig. 5.** The infrared-X-ray spectral energy distribution of Kaz 102 is plotted. The radio-optical photometries are from Elvis et al. (1994), optical spectrum is from de Diego et al. (1998), and X-ray data points are from Fig. 1. The mean RQQ SED from Elvis et al. (1994) is also shown. The SED of an ADAF model is shown for $M_{\text{BH}} = 10^8 M_{\odot}$, $\dot{m} = \dot{m}_{\text{crit}}$ (Di Matteo, priv. comm) is also plotted for comparison. All symbols and line styles are labeled in the figure.

erence to the warm absorber explanation of this object. The best-fit abundance in the warm absorber model using *absori* is still sub-solar (0.1-0.3), which may be too low for a massive system hosting such a luminous QSO. However, it may be possible to explain the X-ray spectrum with higher abundance gas in more complex models, e.g. involving multiple absorber models and/or models involving both the Compton reflection and warm absorber, since having multiple components tend to smooth out edge features, giving a lower abundance when fit with a simple model. Our data cannot make constraints on these complex models and should be a topic of future X-ray observations.

An interesting observation is that we see a soft component at $E < 1.5$ keV during the *ROSAT* observation in 1990, but not during the *Einstein* (1979) and *ASCA* (1999) observations. The difference of the *ROSAT* and *ASCA* spectral slopes in the overlapping energy range far exceeds the reported discrepancy in fitted spectral slopes between these instruments during simultaneous observations of NGC 5548, which suggested spectral response calibration errors in either or both instruments (Iwasawa, Fabian & Nandra 1999). Thus the variability of the soft component cannot be attributed to the cross-calibration problem. Such a variability of the soft component have previously been reported in a number of AGNs including 1H 0419-577 (Guainazzi et al. 1998; Page et al. 2002) and REJ2248-511 (Puchnarewicz et al. 1995). The soft excess component observed by *ROSAT* is not the high energy end of the BBB, which is thought to come from the multi-temperature blackbody emission of the accretion disk. Integrating mid-infrared to ultraviolet SED of Kaz 102 gives a lower limit to its bolometric luminosity $L_{\text{bol}} \gtrsim 2 \times 10^{45} \text{ erg s}^{-2}$, corresponding to an Eddington mass of $\gtrsim 3 \times 10^7 M_{\odot}$. The temperature of the inner ac-

Table 3. Warm Absorber Cloud Parameters

r [cm]	n [cm $^{-3}$]	δr [cm]	v_{cir} [km s $^{-1}$]	t_{cr}
10^{19}	10^5	$10^{18.5}$	400	2000 yr.
10^{18}	10^7	$10^{16.5}$	1000	10 yr.
10^{17}	10^9	$10^{14.5}$	4000	10 days.

cretion disk (assuming non-rotating) around a black hole with this mass is as low as $kT \lesssim 0.02$ keV (e.g. Eq. (12) of Makishima et al. 2000), and thus can very little contribute to the X-ray emission at $E \sim 0.5 - 1$ keV. Page et al. (2002) explains the soft variability of 1H 0419-577 as due to the cooling of comptonizing electrons in the framework of two-temperature coronae and this may also be the case for Kaz 102.

The second interpretation is that the line of sight to the non-thermal continuum is sometimes blocked by the crossing warm absorber cloud. In the framework of the crossing warm absorber picture, we can put order-of-magnitude constraints on the nature of the warm absorbing cloud using the value of $\xi \equiv L_*/nr^2 \approx 200$, where $L_* \approx 2 \times 10^{45}$ erg s $^{-1}$ is the 5eV-300 keV luminosity of the central source irradiating the cloud, estimated from the extrapolation of the unabsorbed power-law component. From the N_{H} of the warm absorber and ξ , we can calculate hydrogen+ion density n and physical depth $\Delta r \approx N_{\text{H}}/n$ of the cloud for a given distance r from the X-ray source. Furthermore, assuming that the central blackhole of $M_{\text{BH}} \sim 10^8 M_{\odot}$ dominate the gravitational force in the region of interest ($r < a$ few pc) and cloud dimensions in depth and width are similar, its circular velocity ($v_{\text{cir}} = GM_{\text{BH}}/r$) and the cloud crossing time ($t_{\text{cr}} = \Delta r/v_{\text{cir}}$) can be estimated. Table 3 shows the results of the calculation. A geometrical constraint $\Delta r < r$ gives $r < 10^{19}$ cm. Taking the crossing warm absorber cloud picture and assuming that t_{cr} is about the timescale of the variability (\lesssim several years), the absorbing cloud is most likely to be located at $r \lesssim 10^{18}$ cm (≈ 0.3 pc) and the value of $v_{\text{cir}} \gtrsim 1000$ kms $^{-1}$ there suggests that it is in the broad-line region.

The third explanation is the change of ionization state of the warm absorber. If the central source was twice as luminous, i.e. ξ increased to 400 (the absorber temperature increases accordingly), the absorber becomes more transparent at $\lesssim 2$ keV, reproducing the steep spectrum of the *ROSAT* observation. However, in the case of Kaz 102, this is not a likely explanation, because the entire spectrum had to be twice as luminous when *ROSAT* observed the soft excess component. It might be possible, however, that *ROSAT* observation was made just after the irradiating source had become fainter, but the absorber retains the previous ionization state. This is not likely the case unless the cloud is located just at the geometrical constraint threshold of $r \approx 10^{19}$ cm with $n \approx 10^5$ cm $^{-3}$ (Table 3). The reason is that Treves et al. (1995) detected no significant variability of the soft X-ray flux ($\lesssim 10\%$ if any) during the repeated *ROSAT* All-Sky Survey scans

through Kaz 102 over ~ 180 days, except for a sign of two brief dips. And the recombination timescale estimated by Eq. (2) of Reynolds & Fabian (1995) is $\approx 10^{12}/n$ s, which become comparable or longer than this timescale only if density is $n \lesssim 10^5$ cm $^{-3}$, hence $r \gtrsim 10^{19}$ cm.

In order to discriminate between the discussed possibilities of the origins of the hard X-ray spectrum and the variability of the soft component, further X-ray observations, including detailed spectral variability study and high resolution spectroscopy such as obtainable with gratings on Chandra/XMM-Newton and the calorimeter on Astro-E2 are needed. After characterizing the physical nature of the object, one can answer the most important question: "Why such AGNs are so rare? Is it just an extreme case of continuous population of type 1 AGNs with warm absorber or is there something essentially different about Kaz 102?"

This work has been partially supported by the NASA Grant NAG-10875 (LTSA) to TM. The authors thank Tiziana Di Matteo for useful discussions on the ADAF possibility and kindly calculating a tailored ADAF SED for this paper. The authors are also thankful to the referee, Kazushi Iwasawa, for various useful comments and pointing to many important references.

References

- Ballantyne D. R., Fabian A. C., Ross R. R. 2002, MNRAS 329, L67
- Cileigi P., Maccacaro T. 1996, MNRAS 282, 477
- de Diego J.A., Dultzin-Hacyan D., Benítez E., Thompson K.L. 1998, A&A 330, 419
- Di Matteo, T. et al. 1999, MNRAS 305, L1
- Di Matteo T., Allen S. W., Fabian A. C., Wilson A. S., Young A. J. 2003, ApJ582, 133
- Done C., Mulchaey J. S., Mushotzky R. F., Arnaud K. A. 1992, ApJ 395, 275
- Elvis M. et al. 1994, ApJS 95, 1
- George I. M. et al., 2000, ApJ 531, 52
- Guainazzi M. et al. 1998, A&A 339, 327
- Page K. L., Pounds K. A., Reeves J. N., O'Brien P. T. 2002, MNRAS 330, L1
- Haardt F., Maraschi L. 1993, ApJ 413, 507
- Iwasawa K., Fabian A.C., Nandra K. 1999, MNRAS 307, 611
- Iwasawa K., Fabian A. C., Almaini O., Lira P., Lawrence A., Hayashida K., Inoue H. 2000, MNRAS318, 879
- Leighly K. M. 1999, ApJS 125, 317
- Magdziarz P., Zdziarski A. 1995, MNRAS 273, 837
- Makishima K. et al. 2000, ApJ 535, 632
- Miyaji, T. 2001 in "Where's the Matter? Tracing Dark and Bright Matter with the New Generation of Large Scale Surveys", eds. Treyer & Tresse (Frontier Group), p357
- Puchnarewicz E. M., Branduardi-Raymont G., Mason K. O., Sekiguchi K. 1995, MNRAS 276, 1281
- Reynolds C. S., Fabian A. C. 1995, MNRAS273, 1167
- Treves, A. et al. 1995, ApJ 442, 589
- Wilkes, B.J. & Elvis, M. 1987, ApJ 323, 243
- Yaqoob T. 2000, ASCA-CAL-00-06-01
(<http://lheawww.gsfc.nasa.gov/~yaqoob/ccd/nhparam.html>)
- Zdziarski A. A., Johnson W. N., Done C., Smith D., McNaron-Brown K. 1995, ApJL 438, L63